Extended Halogen Bonding between Fully Fluorinated Aromatic Molecules

Shigeki Kawai,[*,†,‡] Ali Sadeghi,[†,§] Feng Xu,[⊥] Lifen Peng,[⊥] Akihiro Orita,[⊥] Junzo Otera,[⊥] Stefan Goedecker,[†] and Ernst Meyer[†]

[†]Department of Physics, University of Basel, Klingelbergstrasse 82, CH-4056 Basel, Switzerland, [‡]PRESTO, Japan Science and Technology Agency, 4-1-8 Honcho, Kawaguchi 332-0012, Japan, [§]Department of Physics, Shahid Beheshti University, Evin, 19839 Tehran, Iran, and [⊥]Department of Applied Chemistry, Okayama University of Science, 1-1 Ridai-cho, Kita-ku, Okayama 700-0005, Japan

ABSTRACT Halogen bonding is a noncovalent interaction where an electrophilic cap on a halogen atom, the so-called σ-hole, attracts a nucleophilic site on an adjacent molecule. The polarizability of halogens relates to the strength of the σ-hole, and accordingly the halogen–halogen distance becomes shorter in the order of Cl, Br, and I. Fully fluoro-substituted *aromatic molecules*, on the contrary, are generally believed not to form halogen bonds due to the absence of a σ-hole. Here, we study atomic-scale in-plane F–F contacts with high-resolution force microscopy. Our *ab initio* calculations show that the attractive dispersion forces can overcome the electrostatic repulsion between the fluorine atoms, while the anisotropic distribution of the negative electrostatic potential leads the directional bond and even changes the gap. The coexistence of these two competing forces results in the formation of a "windmill" structure, containing three C–F···F bonds among neighboring molecules. While the σ-hole is absent, the scheme of the C–F···F bonding has a high similarity to halogen bonding.

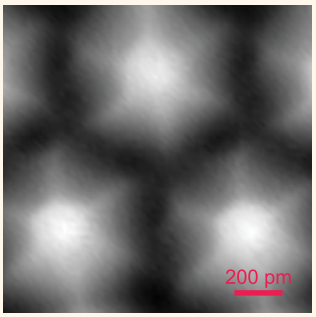

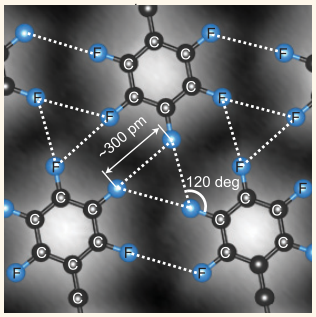

KEYWORDS: intermolecular interaction · chemical structure · F–F contact · halogen bonding · atomic force microscopy

In 1863, Guthrie first reported the ability of halogen atoms to act as an electrophilic component in the synthesis of NH_3I_2 by adding I_2 into a saturated ammonium nitrate solution.[1] This interaction was later identified as halogen bonding, in which an electrophilic terminal halogen moiety noncovalently interacts with a Lewis base.[2] In the last decades, the importance of the halogen bonding in biological systems has been recognized more and more. This bonding can stabilize inter- and intramolecular interactions in proteins and nucleic structures,[3] form four-stranded DNA junctions,[4] transport anions in a lipid layer,[5,6] recognize anions in fluorescence microscopy,[7] and insert a halogen atom inside a molecular container.[8] Halogen bonding has also been utilized in drug design for increased efficiency.[9] In engineering, programmed film structures,[10–17] liquid crystals,[18] and gels[19] can be formed by the halogen bond.

Halogen bonding shares many features with hydrogen bonding, which has been studied much more extensively. In both cases, the electrostatic interaction is responsible for intermolecular interactions. In hydrogen bonding, a partially positively charged hydrogen atom attracts a Lewis base in an adjacent molecule. The directionality of the hydrogen bonding has been established by a number of examples in X-ray analyses.[20] Similarly, a halogen atom attracts a Lewis base, although the mechanism is more complicated. A halogen is intrinsically negatively charged, but when it covalently bonds to another atom (usually carbon) in the molecule, an area of the positive electrostatic potential appears on the outermost portion of the atom along the carbon–halogen bond axis.[21] This anisotropic distribution of the electrostatic potential is responsible for the halogen bond to a Lewis base. Since the positive part, the so-called σ-hole, is localized on the small cap around the atom, the halogen bond is even more directional, compared to the hydrogen bond.[22] The polarizability of the halogen atom, which increases in the order of Cl, Br, and I, relates to the strength

* Address correspondence to shigeki.kawai@unibas.ch.

Received for review October 15, 2014 and accepted February 25, 2015.

Published online February 25, 2015
10.1021/nn505876n

of the σ-hole. Since the belt of the halogen atom still has a negative electrostatic potential, the σ-hole can also bind to the belt of the halogen atom in an adjacent molecule, forming the halogen···halogen bond. However, fluorine has the strongest electronegativity and a low polarizability, so that it *usually* has no σ-hole. The σ-hole is strongly affected by the electron-attracting power, and so, for instance, the cyano moiety behind the C−F bond in FCN[23] and the oxygen in hypofluorite[24] can induce a σ-hole. However, if the electron extraction is not strong enough, F has an intrinsic *negative* electrostatic potential. Simple fluoro-substituted hydrocarbons, such as C_6F_6 and CF_4, are categorized as the latter case. Thus, the halogen bond in such molecules is rarely seen in analyses of crystal structure databases and the stronger C−F···π interaction generally dominates.[25,26] Therefore, analyses of bulk crystal structures cannot reveal the F−F contact. Since, however, the freedom of molecules on a surface is restricted, the in-plane intermolecular interaction at the F−F contact can readily be investigated.

Here, we present clear evidence that an anisotropically distributed negative electrostatic potential around a fluorine atom in a fluoro-substituted aromatic molecule together with a large dispersion force induces a highly directional bonding and gives rise to a well-ordered supramolecular structure on a Ag(111) surface at low temperature. The angle and distance of the bond conformation are directly observed by high-resolution atomic force microscopy (AFM). Furthermore, density functional theory (DFT) calculations show quantitatively the strengths of the competing electrostatic and dispersion forces. This bond has a high similarity to halogen···halogen bonding.

RESULTS AND DISCUSSION

In our experiment, nonsubstituted phenyleneethynylene (bis(4-(phenylethynyl)phenyl)ethyne, BPEPE, Figure 1a) and fully fluoro-substituted phenyleneethynylene (bis(2,3,5,6-tetrafluoro-4-(2,3,4,5,6-pentafluorophenylethynyl)phenyl)-ethyne, BPEPE-F18, Figure 1b) were deposited on a clean Ag(111) surface. Their conformations were analyzed

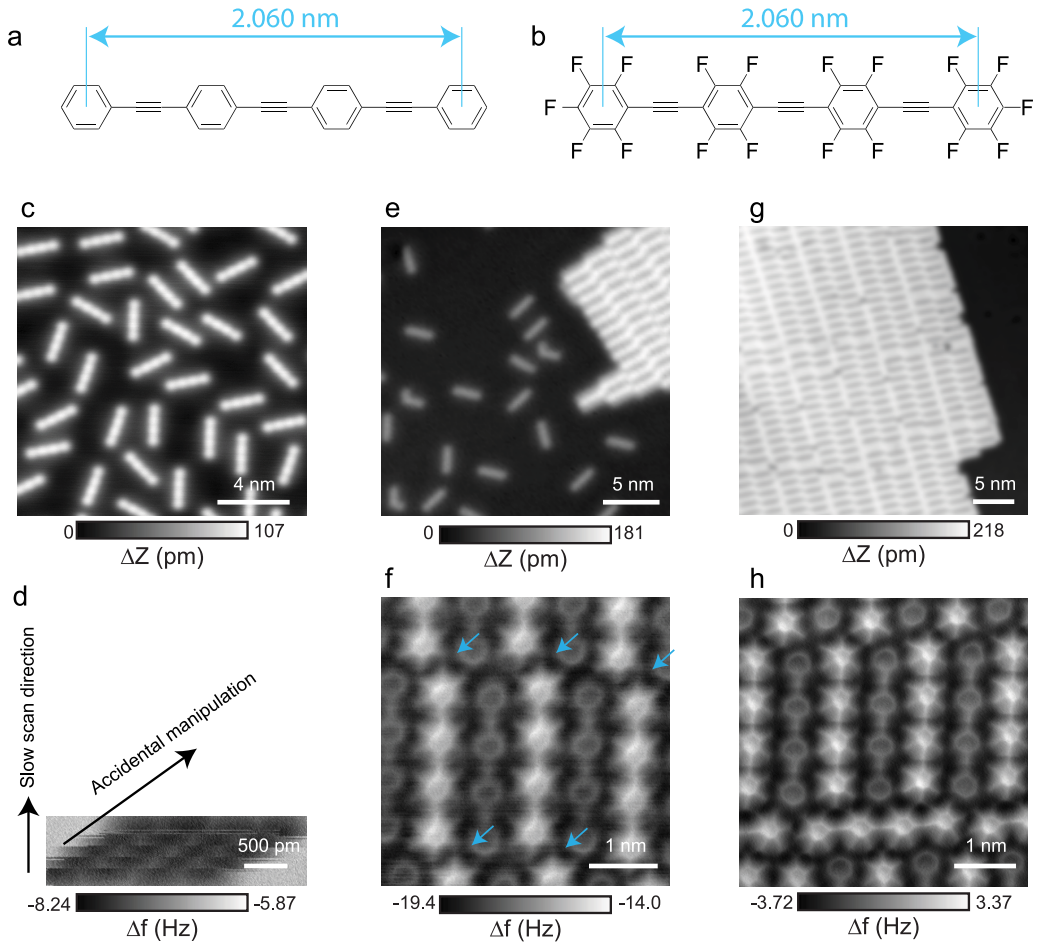

Figure 1. (a, b) Chemical structures of phenyleneethynylenes (BPEPE) and the fully fluoro-substituted phenyleneethynylenes molecule (BPEPE-F18). (c) STM topography of the Ag(111) surface deposited only with BPEPE (0.25 ML). (d) Frequency shift Δf map in a close view. (e) STM topography of the surface with BPEPE (0.12 ML) and a lesser amount of BPEPE-F18 (0.08 ML). (f) Corresponding Δf map, measured at constant height. (g) STM topography of the surface with BPEPE (0.35 ML) and an excess amount of BPEPE-F18 (0.50 ML). (h) Corresponding Δf map, measured at constant height. Measurement parameters: $V_{tip} = -200$ mV and $I = 10$ pA in (c) and $V_{tip} = 200$ mV and $I = 2$ pA in (e) and (g) for STM measurements. $V_{tip} = 0$ mV and $A = 60$ pm for all AFM measurements.

with scanning tunneling microscopy (STM) and AFM at 4.8 K under ultrahigh-vacuum condition.

(Co-)deposition of Non- and Fluoro-substituted Molecules. In order to inspect the intermolecular interactions in the hydrogen−hydrogen contact, we first deposited the nonsubstituted phenyleneethynylene (BPEPE) on a clean Ag(111) surface. In the case of a submonolayer, the molecules have no ordered structure and are individually and randomly adsorbed along six equivalent directions of the Ag(111) surface (Figure 1c). This is due to the fact that the repulsive electrostatic interaction between two molecules is dominating as previously observed with hexa-peri-hexabenzocoronene on Au(111)[27] and free-base porphine on Ag(111).[28] Since long-range molecular orbitals usually affect the STM contrast, a detailed chemical structure can be hard to achieve. Therefore, in order to perform high-resolution imaging, we used AFM, which senses the total electron density of the sample surface.[29] With a CO-terminated tip close to the surface, the chemical structure of molecules can even directly be resolved in the frequency shift map of an oscillating force sensor.[30−32] We attempted to image the chemical structure of BPEPE with AFM, but it was laterally moved by the tip−sample interaction before the tip approaches the repulsive region (Figure 1d). This result indicates the small corrugation amplitude of potential on the Ag(111) surface. Therefore, resolving the chemical structure was not possible.

Consequently, we co-deposited excess BPEPE and, to a lesser extent, BPEPE-F18. Figure 1d shows the STM topography. At the left-hand side, the residual BPEPEs are adsorbed individually, as observed in Figure 1c. We observed a well-ordered supramolecular structure at the right-hand side. The brighter and darker contrasts correspond to BPEPE-F18 and BPEPE, respectively. The two kinds of molecules are alternatively aligned, and the weak C−F···H hydrogen bonding (attractive interaction) is responsible for the assembly.[33,34] Since the supramolecular structure increases the stability of the individual molecule, the molecules were no longer manipulated by the CO-terminated tip with a conventional tip−sample separation for imaging chemical structures of molecules (Figure 1f). Due to the effect of the tilting CO molecule, the benzenes of BPEPE are observed as distorted and larger.[32] In contrast, due to the different extents of their π-electrons,[35] the fluorobenzenes are observed smaller and brighter. Although the actual positions of the atomic cores in the molecule cannot be imaged directly, the atomic-scale arrangements of BPEPE and BPEPE-F18 are clearly observed. In addition to the C−F···H hydrogen bonding, C−F···F−C bondings are also observed as indicated with arrows. Next, we co-deposited BPEPE and excess BPEPE-F18. A well-ordered molecular film was again observed (Figure 1g), but in this case, no residual BPEPE nor BPEPE-F18 was observed on the terrace because all BPEPE and BPEPE-F18 are incorporated into the self-assembly by C−F···H hydrogen bonding. Further, the number of C−F···F−C bondings in the supramolecular structure increases (Figure 1h), yet it is not conclusive evidence for whether C−F···F−C bondings increase the stability of the supramolecular structure or not.

Apparent Intermolecular Bond. We observed an interesting bond-like feature in the C−F···F−C contact. Zhang *et al.* reported in 2013 that the hydrogen bondings can be resolved by a CO-functionalized tip of AFM, similar to the intramolecular covalent bonds.[36] The explanation put forward in their article is that the partially covalent nature of the hydrogen bond increases the electron density,[20] and hence the bond site has a stronger Pauli repulsion. More recently Hapala *et al.* claimed that the increased electron density is not sufficient for the contrast; rather the landscape of the potential energy in the adjacent atoms is responsible. Thus, they claimed that *sharp apparent intermolecular bonds should not be interpreted as true hydrogen bonds*.[37] Very recently, the conclusive study to support the argument of Hapala *et al.* was presented *via* the experimental and theoretical studies of hydrogen bonding.[38] Nevertheless, since our F−F intermolecular interaction is purely of electrostatic nature, the increased electron density is absent. For this reason, it is ideal to examine the topic. Figure 2a shows the conformations of BPEPE and BPEPE-F18 (Figure 1h repeated for convenience). In order to emphasize the contrast, we applied Laplace filtering to the image (Figure 2b). The different orders of intramolecular bond are clearly visible. In addition, we observe the intermolecular bonds in the F−F contact. Figure 2c and d show the magnified views of the Δf and corresponding Laplace filtered image, respectively. Although no shared electron exists in the C−F···F−C contact (as calculated in Figure 4b), apparent intermolecular bonds are clearly observed. This is an indirect evidence that the observed bond-like feature does not relate to any intermolecular bond, but rather the tilting of the CO molecule on the tip by the landscape of the potential, as reported by Hapala *et al.*[37] and Hämäläinen *et al.*[38]

Atomic-Scale Imaging of Organic Fluorine Contact. In order to investigate the C−F···F−C interaction, we deposited only BPEPE-F18. In contrast to BPEPE, a well-ordered supramolecular assembly was formed with BPEPE-F18 (Figure 3a), indicating that C−F···F−C bonding observed in Figure 1h is attractive. The structure grew in the [2$\bar{3}$1] direction, and its domain extended on the terrace of Ag(111) up to 100 nm × 100 nm. The inset shows the close-up view of the molecules. The four observed protrusions in the STM topography correspond to the benzene rings; the two rings at the ends appear higher than the central two at an applied bias voltage of −200 mV.

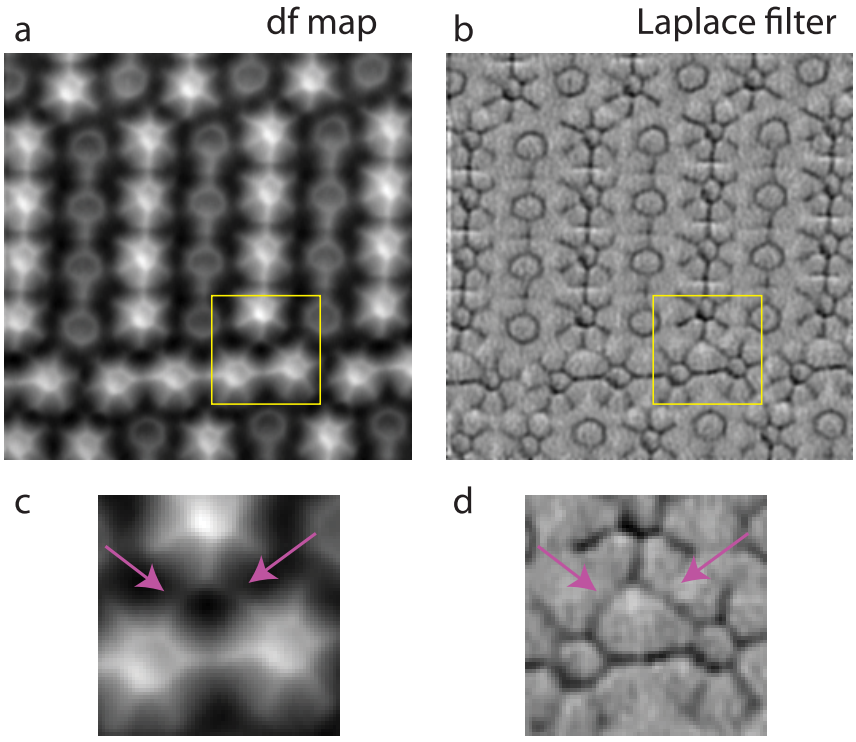

Figure 2. (a) Δf map. (b) Corresponding Laplace filtered Δf map. (c) Magnified image at the area indicated by a broken box in (a). (d) Corresponding Laplace filtered Δf map.

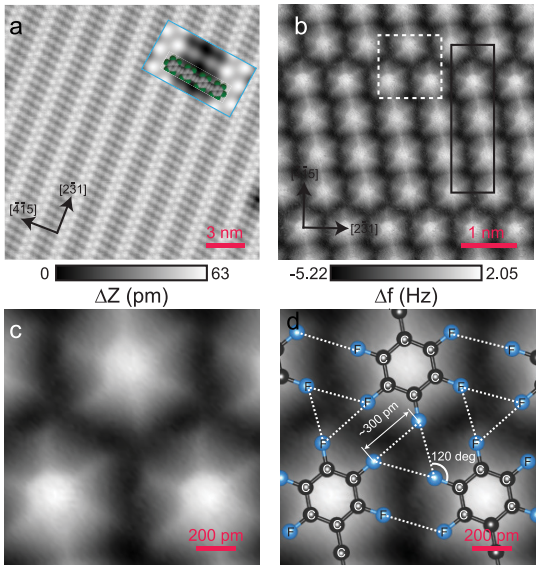

Figure 3. (a) Scanning tunneling microscopy (STM) topography of the self-assembled BPEPE-F18 molecules on Ag(111). The inset shows the magnified image after mesh-averaged filtering. (b) Frequency shift Δf map of the self-assembly, taken with a carbon-monoxide-terminated tip at a constant height mode. The unit cell is shown by a black rectangle. (c) Magnified Δf map, indicated by a white square in (d). (d) Same as (c) with a superimposed stick-and-ball drawing of the molecules. Measurement parameters: bias voltage V_{tip} = −200 mV and tunneling current I = 10 pA in (a) and V_{tip} = 0 mV and oscillation amplitude A = 60 pm in (b).

Figure 3b shows the frequency shift map of the film, obtained with a CO tip. In contrast to the STM topography, all four benzene rings appear with almost the same contrast, which implies that the molecule lies flat on the surface. The molecular axis is an almost perfect straight line, even though the phenyleneethynylene array is somewhat flexible.[33] Therefore, the difference in the apparent height in the STM topography (Figure 3a) is associated with the orbitals localized on the pentafluorobenzene moieties (Supporting Information). Since no other structure of assembly was observed, this conformation would be energetically the most stable. Our interest was immediately focused on the intermolecular interactions. In order to obtain a higher signal-to-noise ratio, the image was mesh-averaged over the unit cell.[39] Then, the area indicated by a square box in Figure 3b was magnified (Figure 3c). The hexagonal benzene rings and the C—F bonds are clearly observed.

As described above, since the apparent intermolecular bond is subject to the complex imaging mechanism (tilting CO tip and the potential landscape),[37] it is not trivial to assign the bond length and angle directly from the observed AFM image. Further, the effect of the CO tip tilt is sensitive enough to detect the bond order[32] and extended electronic cloud.[35] In other words, the actual positions of atomic cores cannot be measured directly from the AFM image. Therefore, we first assigned the chemical structure of the molecule with the know dimension of BPEPE-F18 (Figure 1b, length: 20.60 Å, C—F: 1.34 Å, and C—F: 1.39 Å) to the observed molecule and then analyzed the bond length and angle. As indicated with broken white lines (Figure 3d), each C—F bond points to a fluorine atom

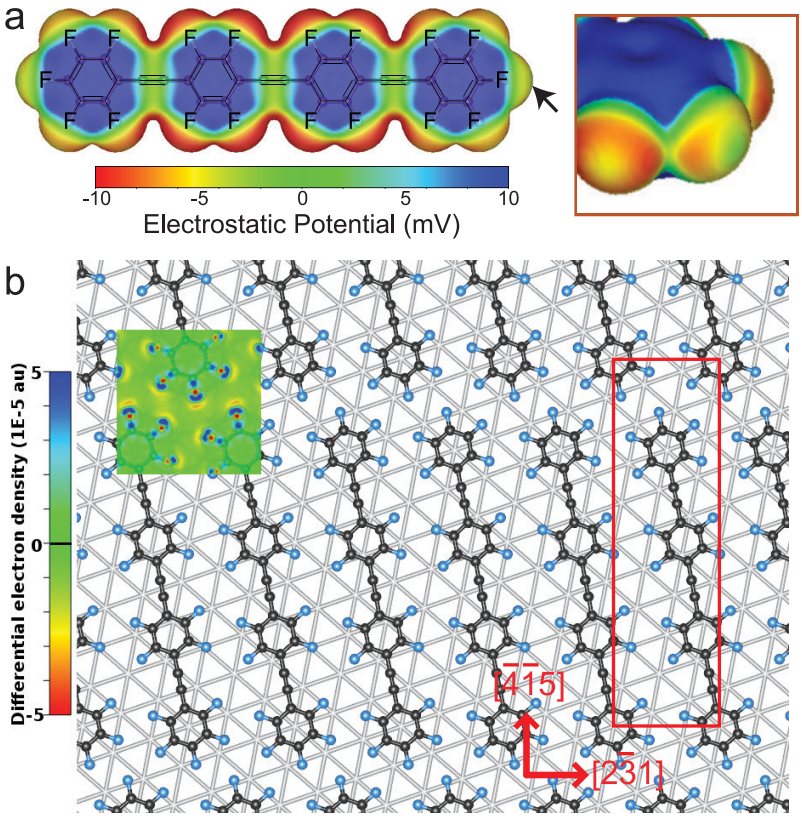

Figure 4. (a) Calculated molecular electrostatic potentials of BPEPE-F18 projected on the constant density (0.001 e/Bohr^3) surface. (b) Schematic drawing of the position of the molecular layer over Ag(111), calculated with DFT. The top layer of the substrate is indicated with white circles, and C and F atoms are shown with black and blue circles. The unit cell of the assembly is shown by a red box, and the arrows indicate the crystallographic directions of the substrate. Inset: Differential electron density (e/Bohr^3) of the self-assembly, showing electron depletion (yellow) outside the molecule as an indication of repulsive electrostatic interaction.

in the adjacent molecule, which results in highly directional C—F···F bonds (~180 deg). Furthermore, the angles between the C—F···F bonds are approximately 120 deg, resulting in the formation of an inverted "windmill" structure. All F—F contacts in Figure 3d have *almost* the same bond lengths and angles. Similar directional bondings in the X—X contacts (X = Cl, Br, and I) have been reported,[10−17,40] where the lengths of the halogen bonds are shorter than the sum of the van der Waals (vdW) radii due to the halogen···halogen bonding. However, in the present case, the measured F···F bond length (broken white lines) is at least 300 pm, *i.e.*, slightly larger than twice the vdW radius of a fluorine atom (*i.e.*, 294 pm), indicating the coexistence of a repulsive interaction. This large distance is a clear evidence that this bond differs from the typical halogen···halogen bonding observed before. A similarly packed structure was also observed with tetrafluoromethane (Supporting Information).

Electrostatic Potential Analysis. First, we attempted to understand the mechanism of the directional C—F···F bonding, based on the commonly used electrostatic potential analysis.[21] Figure 4a shows the calculated molecular electrostatic potential (MEP) of BPEPE-F18 on a constant electron density surface (0.001 e/Bohr^3).[41] Because of the high electronegativity of fluorine, DPEPE-F18 has a positive MEP at the center of benzenes, enabling it to serve as an electron-accepting material such as an n-type semiconductor, while on the outer shell of DPEPE-F18 the MEP turns negative.[42,43] In a detailed inspection (right panel of Figure 4a), the MEP on the fluorine atom varies and the cap has the least negative value. However, since no positive part appears (no σ-hole), the electrostatic interaction in the F—F contact is always repulsive. Therefore, the analysis in terms of the electrostatic potential is not sufficient to explain the observed directional C—F··· F bonding in contrast to the case of other heavier halogen atoms such as Cl and Br (Supporting Information).

Next, we performed a series of extensive periodic DFT calculations, including both the molecules and the substrate. We used the PBE functional together with empirical vdW corrections,[44] which is widely used for this kind of analysis (for details, see the Methods section). Figure 4b depicts the relaxed conformation of BPEPE-F18 in the molecular film on the Ag(111) surface. Since the conformation of the supramolecular structure is commensurate with the substrate lattice, the centers of the pentafluorobenzene moieties are

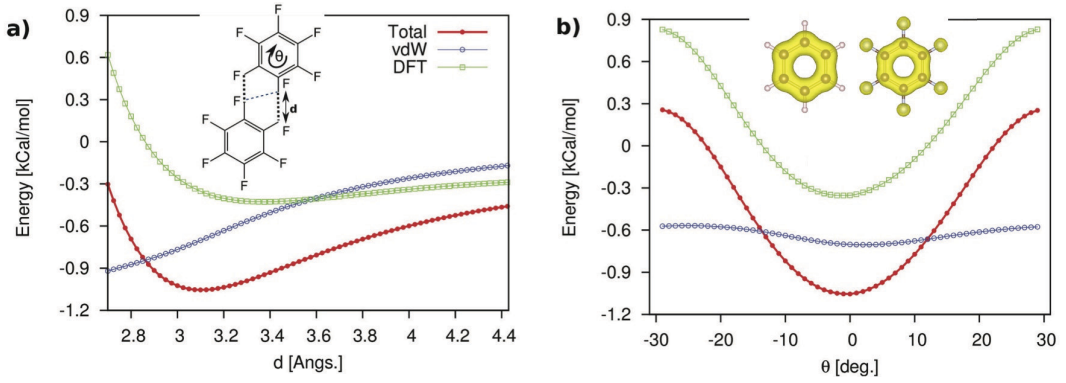

Figure 5. (a) Total cohesive energy and its contributions (vdW: van der Waals, DFT: electrostatic interaction from charge density obtained by the DFT calculation) for two hexafluorobenzenes C_6F_6 as a function of the distance *d* between F atoms. The inset illustrates the definition of *d* and θ. One kcal/mol = 0.043 eV. (b) Same as (a) but for a rotation of one molecule around its normal axis going through the center of the hexagon of carbon atoms at a constant distance of *d* = 3.1 Å between the two molecules. The rotation angle $\theta = 0$ corresponds to the shown configuration, *i.e.*, C−F···F along a straight line. The inset illustrates that the π-electronic density surface (0.005 au) remains angle-independent over carbon atoms in both C_6H_6 (left) and C_6F_6 (right).

located on the equivalent silver sites and equilateral triangles are formed by three straight C−F···F bonds in the contact. In agreement with the observed AFM image (Figure 3b), the molecule is almost flat (~4 pm) because the vdW force is dominant in the molecule−substrate interaction [physisorption with a binding energy of −84 kcal/mol (−3.6 eV) for each molecule]. To verify that the molecule−substrate interaction plays no significant role in the supramolecular network structure, we additionally relaxed the atomic positions and unit cell of the freestanding molecular layer. The layer preserves its structure in the absence of the substrate with a cohesive energy of −5.9 kcal/mol (−260 meV). The inset of Figure 4b shows the change of the electron density induced by the self-assembly. Although the adjacent molecules attract each other in total, the electron depletion outside the molecules (yellow region) implies an electrostatic repulsion at the F−F contacts. In fact, the electrostatic potential around F atoms in contact becomes more negative (Supporting Information). This, again, shows that the common description of the halogen bonding based on an *attractive* electrostatic interaction cannot be applied to this fluorine contact case.

Analysis of Directional Halogen Bond. To investigate the directionality of the bond in detail, two isolated hexafluorobenzenes (HFBs) are considered. After the relaxation of the isolated HFBs, one of the HFBs is rigidly moved along to the C−F···F bonds toward the other. Figure 5a shows the variation of the cohesive energy as a function of the F−F distance *d* (see inset of Figure 5a). The total cohesive energy, including electrostatic and vdW contributions, has a minimum at *d* = 3.1 Å, which is virtually identical to the separation of the HFB rings in neighboring BPEPE-F18 molecules on the silver surface. Since the vdW contribution, missing in DFT energies, is added empirically and the charge distribution is not affected by vdW interactions, it is possible to separate out the vdW contribution in our simulation. Such a separation was done in a different way in a previous work for the attractive R−X···Lewis base halogen bonding (X = Cl, Br).[45] Both methods should give a very good estimation of the vdW energies. The pure electrostatic energy difference has mainly repulsive character. It is obtained *via* the Hellmann−Feynman theorem, which states that the forces acting on the nuclei arise from the electronic charge distribution. Integrating the Hellmann−Feynman forces along the displacement path therefore gives this energy difference. Note that our calculations do not suffer from errors due to incompleteness of the basis set, and therefore Pulay corrections are not needed because the calculated electron density is extremely accurate.

Now, if one HFB is rigidly rotated around its normal axis (the C_6 axis) while the other one is kept at the equilibrium distance (see inset of Figure 5a), the vdW energy varies only slightly. This can be explained in terms of the very low polarizability of fluorine, while the electron clouds made from the carbon π-orbitals of each HFB are polarizable and therefore have strong vdW interactions. Since the spatial distribution of the π-cloud is nearly independent of the rotation angle (see inset of Figure 5b), the vdW energy changes only marginally when θ is varied. On this basis, we argue that the deep minimum of the energy *versus* θ curve, *i.e.*, the high directionality of the C−F···F bond, originates from the F−F *electrostatic* interactions. Likewise in the commonly known X−X halogen bonding (X = Cl, Br, I), the energy minimum occurs when the three atoms in C−F···F are positioned on a straight line, *i.e.*, when the cap of one F points toward the belt of the other one. Note that the strong electron attraction of the halogenated carbon atom, as evidenced by the less negative potential at the cap of fluorine, plays a crucial role, whereas the intrinsically strong electrostatic repulsion between two spherically symmetric F^- ions prevents bonding (the Coulomb

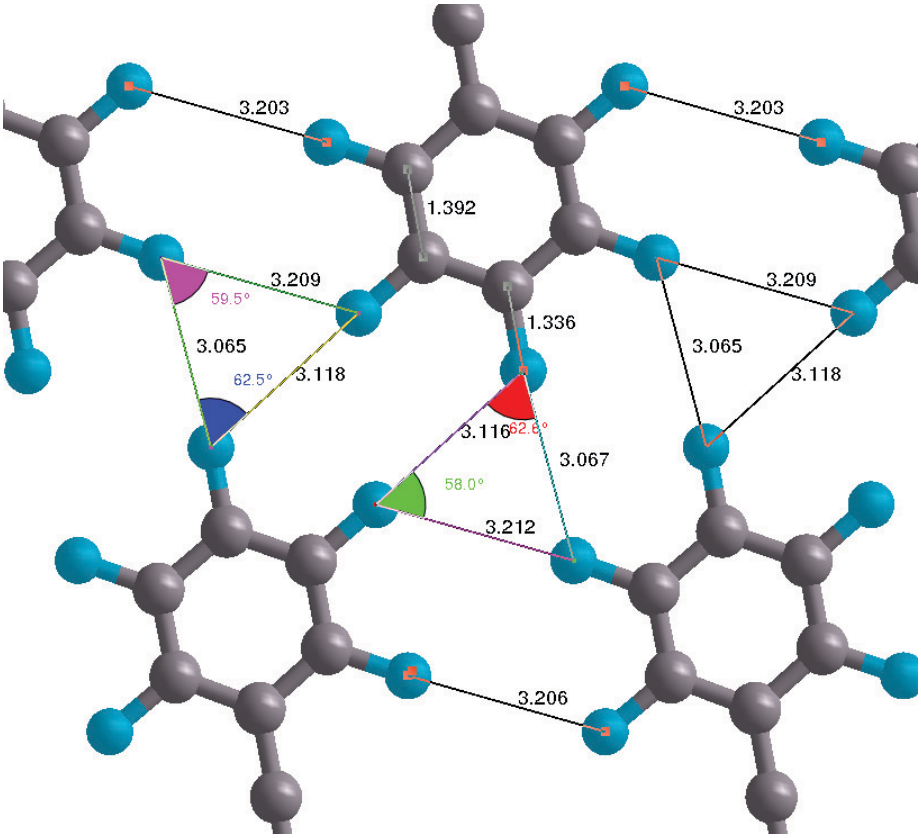

Figure 6. Calculated geometrical properties of the BPEPE-F18 molecular layer. (*cf.* Figure 3b). Intra- and intermolecular distances are given in angstrom, and angles in degree.

repulsion between two F^- separated by 3.1 Å is 108 kcal/mol (4.7 eV); from DFT it is 99 kcal/mol (4.3 eV)). The influence of the less negative cap can be seen *via* the different C−F···F bond lengths. The electron attraction of the halogenated carbon atom along the molecular axis is stronger than others due to the imbalanced charge distribution, so that the F cap has the least negative potential compared to the other F caps, as shown in Figure 4a. Thus, the length of the C−F···F bond along the molecular axis is the smallest due to the smaller electrostatic repulsion. In order to investigate this influence, the geometrical details of the molecular structure, based on our DFT calculations, is presented in Figure 6. We found that the C−F bonds vary, depending on the molecular site, while the C−C bond length is almost constant (139 pm). This is due to the fact that the electron attraction by the halogenated carbon atom is tuned by the imbalance of the charge distribution in the pentafluorobenzene moiety. This strong electron attraction of the C−F bond along the molecular axis results in the least negative potential at the F cap (Supporting Information). Therefore, the electrostatic repulsion in the C−F···F contact along the molecular axis becomes smaller, so that the bond length (307 pm) becomes longer compared to the others (321 pm).

This delicate balance of competing electrostatic and vdW forces gives rise to the C−F···F bond. This bond has a high similarity to the halogen−halogen bonding but is weaker than the others since the σ-hole is absent. Further, through the inspection of Figures 1 and 3, the C−F···F−C bond is weaker than the weak C−F···H hydrogen bond; otherwise a condensed BPEPE-F18 domain would have appeared in Figure 1g. This observation is in good agreement with the calculation. The total cohesive energy in two hexafluorobenzenes is −1.06 kcal/mol (−46 meV, Figure 5b). This contact is composed of two C−F···F−C halogen bondings and so that each energy is approximately −0.53 kcal/mol (−23 meV), which is half of that of the C−F···H−C hydrogen bonding (−1.08 kcal/mol (−47 meV)).[25] Thus, C−F···H−C hydrogen bonding is more preferential in the compounds as found in the crystal analysis.[46] The existence of the C−F···F bonding can experimentally also be deduced from the fact that the nonsubstituted molecules do not self-assemble because the dispersion interaction is not strong enough to overcome the electrostatic repulsion.

Finally, we address the charge transfer between organic molecules and a metallic substrate, which can induce significant change on the electrostatic interaction between adjacent molecules. To this aim, the Bader definition[41] was employed to determine the splitting border between the molecules and substrate. The charges, transferred to each of the non- and

F-substituted molecules, turn out to be −0.12 and −0.63 e, respectively. Since vdW interactions are directly related to the molecular polarizability, the extra charge would strengthen or weaken the vdW interactions at the end. Therefore, we calculated the molecular polarizability for both neutral and charged free molecules along the molecule axis (α_{xx}). We obtained α_{xx} = 1432 and α_{xx} = 1585 for the nonsubstituted molecule and neutral F-substituted molecules in atomic units, respectively. Once the above-mentioned fractional charges are added to the molecules, those values increase by 28% and 32%, respectively. Therefore, one expects that the vdW attraction becomes even stronger than that predicted by the empirical method of Grimme for neutral molecules, which helps to condense BPEPE-F18. However, the increased vdW is still not strong enough to condense BPEPE as previously discussed in refs 27 and 28.

CONCLUSION

In summary, we reported an atomic-scale fluorine homocontact of fully fluoro-substituted aromatic molecules, which induces a two-dimensional supramolecular structure on the Ag(111) surface. The complex chemical structure is directly revealed by high-resolution atomic force microscopy, clearly showing that the directional bonding exists in an organic fluorine contact. The dispersion force takes the major part in the attraction, but the driving force of the directional bonding is due to the anisotropically distributed electrostatic potential around the fluorine atoms. The geometrical conformations of the molecule on the substrate, obtained by dispersion-corrected density functional calculations, are in perfect agreement with the experimentally observed structures. Furthermore, the contributions from each of the two competing interactions to the cohesive energy of the layer were calculated. Our system illustrates well that dispersion forces can play a decisive role in the formation of ordered supramolecular structures. Our interpretation can be applied to the previously observed fluoro-substituted molecular film by scanning tunneling microscopy with submolecular resolution[47] and the in-plane molecular interaction of π-stacked perfluoropentacene.[48] The reported C−F···F bonding has a high similarity to halogen−halogen bonding in terms of the directionality and influence of the anisotropically distributed electrostatic potential on F and can be categorized as halogen−halogen bonding.

METHODS

AFM Measurements. All measurements were performed with a commercially available Omicron low-temperature STM/AFM system, operating in ultrahigh vacuum at 4.8 K. We used a tuning fork with a chemically etched tungsten tip as a force sensor.[49] The resonance frequency and the mechanical quality factor are 24 803.5 Hz and 18 648, respectively. The high stiffness of 1800 N/m realizes a stable operation with a small amplitude of 60 pm,[50] which was calibrated by the current control method.[51] The small-amplitude operation enhances the detection sensitivity to the short-range tip−sample interaction, and hence the spatial resolution can be improved. The frequency shift, caused by the tip−sample interaction, was detected with a commercially available digital phase-locked loop (Nanonis: OC-4 and Zurich Instruments: HF2-LI and HF2-PLL).[52] In order to avoid cross-talk between the STM and AFM detection lines, the tungsten tip was electrically decoupled to the detection line of the tuning fork sensor oscillation with a separate Au wire.[53] In the measurement, no significant correlation between the energy dissipation and tunneling current signals was detected. For the STM measurement, the bias voltage was applied to the tip while the sample was electronically grounded. The tip apex was *ex situ* sharpened by milling with a focused ion beam. The tip radius was less than 10 nm. A clean silver tip was *in situ* formed by indenting the Ag sample surface and applying a pulse bias voltage between the tip and sample several times. For AFM, the tip apex was terminated with a CO molecule, which was picked up from the surface.[54] A clean Ag(111) surface was *in situ* prepared by repeated cycles of standard Ar^+ sputtering (3×10^{-6} mbar, 1000 eV, and 15 min) and annealing at 480 °C. The typical width of the Ag(111) terrace was more than 200 nm. In this experiment, we used bis(2,3,5,6-tetrafluoro-4-(2,3,4,5,6-pentafluorophenylethynyl)phenyl)ethyne (BPEPE-F18) and bis(4-(phenylethynyl)phenyl)ethyne (BPEPE).[55] BPEPE-F18 and BPEPE were deposited on the surfaces from crucibles of a Knudsen cell, heated at 145 °C after degassing at 100 °C for several days. The substrate was kept at room temperature. Measured images were analyzed using the WSxM software.[56]

Theoretical Calculations. The periodic *ab initio* calculations were carried out within the generalized gradient approximation of DFT using the VASP code.[57−60] For the molecules, we used the BigDFT code[61] using a wavelet basis set with a grid spacing of 0.17 Bohr and HGH pseudopotentials.[62,63] As valence electrons of C, F, and Ag, we considered the $2s^2 2p^2$, $2s^2 s^2 2p^5$, and $3s^1 4d^{10}$ electrons, respectively. The wave functions were expanded using a plane-wave basis with a kinetic energy cutoff of 400 eV. The core electrons were eliminated using the projector-augmented wave (PAW) method.[64,65] Dispersion effects were treated with the DFT-D2 method of Grimme,[44] where the C_6 parameters were set to 24.67, 1.75, 0.75, and 0.14 and R_0 to 1.639, 1.452, 1.287, and 1.001 for Ag, C, F, and H atoms, respectively. The Ag(111) surface was modeled by a four-layer slab of 112 atoms in total. An orthorhombic supercell ($0.775 \times 2.68 \times 2.2$ nm^3) was used; the lateral edges (along $[2\bar{3}1]$ and $[\bar{4}15]$) coincide with the lattice vectors of the molecular layer, while the third one (along [111]) was chosen such that a vacuum not thiner than 1.2 nm separates the repeated images of the Ag slab. Two atomic layers at the bottom were kept frozen in their bulk position, while all other atoms were allowed to relax until the force on each atom became smaller than 0.02 eV/Å. The reciprocal space was sampled using a $4 \times 2 \times 1$ *k*-mesh. For visualizing the atomic structures V_Sim[66] and VESTA[67] were used.

Conflict of Interest: The authors declare no competing financial interest.

Acknowledgment. This work was supported in part by the Japan Science and Technology Agency (JST) "Precursory Research for Embryonic Science and Technology (PRESTO)" for the project "Molecular technology and creation of new function", by the Swiss National Science Foundation, by the NCCR "Nanoscale Science" of the Swiss National Science Foundation, by a matching fund subsidy for private universities from the Ministry of Education, Culture, Sports, Science and Technology, Japan, by the Japan Society for the Promotion of Science (JSPS) through its "Funding Program for World-Leading Innovative R&D on Science and Technology (FIRST Program)", and by

Okayama Prefecture Industrial Promotion Foundation. S.K. thanks Leo Gross, Bruno Schuler, and Gerhard Meyer for valuable discussions and Marcel Düggelin for preparation of the tip by a focused ion beam. A.S. thanks Ali Talebi for fruitful discussions. The computing time was provided by CSCS.

Supporting Information Available: Scanning tunneling microscopy image contrast of BPEPE-F18, tetrafluoromethane assembly, molecular electrostatic potentials of BPEPE and BPEPE-X18 (X = F, Cl, and Br), and increased negative electrostatic potential by molecular contact are discussed. This material is available free of charge *via* the Internet at http://pubs.acs.org.

REFERENCES AND NOTES

1. Guthrie, F. XXVIII.-On the Iodide of Iodammonium-. *J. Chem. Soc.* **1863**, *16*, 239–244.
2. Hassel, O. Structural Aspects of Interatomic Charge-Transfer Bonding. *Science* **1970**, *170*, 497–502.
3. Auffinger, P.; Hays, F. A.; Westhof, E.; Ho, P. S. Halogen Bonds in Biological Molecules. *Proc. Natl. Acad. Sci. U.S.A.* **2004**, *101*, 16789–16794.
4. Voth, A. R.; Hays, F. A.; Ho, P. S. Directing Macromolecular Conformation through Halogen Bonds. *Proc. Natl. Acad. Sci. U.S.A.* **2007**, *104*, 6188–6193.
5. Jentzsch, A. V.; Emery, D.; Metrangolo, J. M. P.; Resnati, G.; Matile, S. Ditopic Ion Transport Systems: Anion-π Interactions and Halogen Bonds at Work. *Angew. Chem., Int. Ed.* **2011**, *50*, 11675–11678.
6. Jentzsch, A. V.; Emery, D.; Mareda, J.; Nayak, S. K.; Metrangolo, P.; Resnati, G.; Sakai, N.; Matile, S. Transmembrane Anion Transport Mediated by Halogen-Bond Donors. *Nat. Commun.* **2012**, *3*, 905.
7. Caballero, A.; Zapata, F.; White, N. G.; Costa, P. J.; Félix, V.; Beer, P. D. A. Halogen-Bonding Catenane for Anion Recognition and Sensing. *Angew. Chem., Int. Ed.* **2012**, *51*, 1876–1880.
8. El-Sheshtawy, H. S.; Bassil, B. S.; Assaf, K. I.; Kortz, U.; Nau, W. M. Halogen Bonding inside a Molecular Container. *J. Am. Chem. Soc.* **2012**, *134*, 19935–19941.
9. Lu, Y.; Shi, T.; Wang, Y.; Yang, H.; Yan, X.; Luo, X.; Jiang, H.; Zhu, W. Halogen Bonding-A Novel Interaction for Rational Drug Design? *J. Med. Chem.* **2009**, *52*, 2854–2862.
10. Koudia, M.; Abel, M.; Maurel, C.; Bliek, A.; Catalin, D.; Mossoyan, M.; Mossoyan, J.-C.; Porte, L. Influence of Chlorine Substitution on the Self-Assembly of Zinc Phthalocyanine. *J. Phys. Chem. B* **2006**, *110*, 10058–10062.
11. Gutzler, R.; Ivasenko, O.; Fu, C.; Brusso, J. L.; Rosei, F.; Perepichk, D. F. Halogen Bonds as Stabilizing Interactions in a Chiral Self-Assembled Molecular Monolayer. *Chem. Commun.* **2011**, *47*, 9453–9455.
12. Chung, K.-H.; Park, J.; Kim, K. Y.; Yoon, J. K.; Kim, H.; Han, S.; Kahng, S.-J. Polymorphic Porous Supramolecular Networks Mediated by Halogen Bonds on Ag(111). *Chem. Commun.* **2011**, *47*, 11492–11494.
13. Gutzler, R.; Fu, C.; Dadvand, A.; Hua, Y.; MacLeod, J. M.; Rosei, F.; Perepichka, D. F. Halogen Bonds in 2D Supramolecular Self-Assembly of Organic Semiconductors. *Nanocale* **2012**, *4*, 5965–5971.
14. Noh, S.-K.; Jeon, J. H.; Jang, W. J.; Kim, H.; Lee, S.-H.; Lee, M. W.; Lee, J.; Han, S.; Kahng, S.-J. Supramolecular Cl···H and O···H Interactions in Self-Assembled 1.5-Dichloroanthraquinone Layers on Au(111). *ChemPhysChem* **2013**, *14*, 1177–1181.
15. Silly, F. Selecting Two-Dimensional Halogen-Halogen Bonded Self-Assembled 1,3,5-Tris(4-iodophenyl)benzene Porous Nanoarchitectures at the Solid-Liquid Interface. *J. Phys. Chem. C* **2013**, *117*, 20244–20249.
16. Zha, B.; Miao, X.; Liu, P.; Wu, Y.; Deng, W. Concentration Dependent Halogen-Bond Density in the 2D Self-Assembly of a Thienophenanthrene Derivative at the Aliphatic Acid/Graphite Interface. *Chem. Commun.* **2014**, *50*, 9003–9006.
17. Pham,T. A.; Song, F.; Nguyen, M.-T.; Stöhr, M. Self-Assembly of Pyrene Derivatives on Au(111): Substituent Effects on Intermolecular Interactions. *Chem. Commun.* **2014**, *50*, 14089.
18. Nguyen, H. L.; Horton, P. N.; Hursthouse, M. B.; Legon, A. C.; Bruce, D. W. Halogen Bonding: A New Interaction for Liquid Crystal Formation. *J. Am. Chem. Soc.* **2004**, *126*, 16–17.
19. Meazza, L.; Foster, J. A.; Fucke, K.; Metrangolo, P.; Resnati, G.; Steed, J. W. Halogen-Bonding-Triggered Supramolecular Gel Formation. *Nat. Chem.* **2013**, *5*, 42–47.
20. Steiner, T. The Hydrogen Bond in the Solid State. *Angew. Chem., Int. Ed.* **2002**, *41*, 48–76.
21. Clark, T.; Hennemann, M.; Murray, J. S.; Politzer, P. Halogen Bonding: the σ-Hole. *J. Mol. Model.* **2007**, *13*, 291–296.
22. Voth, A. R.; Khuu, P.; Oishi, K.; Ho, P. S. Halogen Bonds as Orthogonal Molecular Interactions to Hydrogen Bonds. *Nat. Chem.* **2009**, *1*, 74–79.
23. Politzer, P.; Murray, J. S.; Concha, M. C. Halogen Bonding and the Design of New Materials: Organic Bromides, Chlorides and Perhaps Even Fluorides as Donors. *J. Mol. Model.* **2007**, *13*, 643–650.
24. Metrangolo, P.; Murray, J. S.; Pilati, T.; Politzer, P.; Resnati, G.; Terraneo, G. Fluorine-Centered Halogen Bonding: A Factor in Recognition Phenomena and Reactivity. *Cryst. Growth Des.* **2011**, *11*, 4238–4246.
25. Reichenbächer, K.; Süss, H. I.; Hulliger, J. Fluorine in Crystal Engineering-"the Little Atom That Could". *Chem. Soc. Rev.* **2005**, *34*, 22–30.
26. Politzer, P.; Murray, J. S. Halogen Bonding: An Interim Discussion. *ChemPhysChem* **2013**, *14*, 278–294.
27. Wagner, C.; Kasemann, D.; Golnik, C.; Forker, R.; Esslinger, M.; Müllen, K.; Fritz, T. Repulsion between Molecules on a Metal: Monolayers and Submonolayers of Hexa-Peri-Hexabenzocoronene on Au(111). *Phys. Rev. B* **2010**, *81*, 035423.
28. Bischoff, F.; Seufert, K.; Auwürter, W.; Joshi, S.; Vijayaraghavan, S.; Écija, D.; Diller, K.; Papageorgiou, A. C.; Fischer, S.; Allegretti, F.; *et al*. How Surface Bonding and Repulsive Interactions Cause Phase Transformations: Ordering of a Prototype Macrocyclic Compound on Ag(111). *ACS Nano* **2013**, *7*, 3139–3149.
29. Moll, N.; Gross, L.; Mohn, F.; Curioni, A.; Meyer, G. A. Simple Model of Molecular Imaging with Noncontact Atomic Force Microscopy. *New J. Phys.* **2012**, *14*, 083023.
30. Gross, L.; Mohn, F.; Moll, N.; Liljeroth, P.; Meyer, G. The Chemical Structure of a Molecule Resolved by Atomic Force Microscopy. *Science* **2009**, *325*, 1110–1114.
31. Gross, L.; Mohn, F.; Moll, N.; Meyer, G.; Ebel, R.; Abdel-Mageed, W. M.; Jaspars, M. Organic Structure Determination Using Atomic-Resolution Scanning Probe Microscopy. *Nat. Chem.* **2010**, *2*, 821–825.
32. Gross, L.; Mohn, F.; Moll, N.; Schuler, B.; Criado, A.; Guitián, E.; Peña, D.; Gourdon, A.; Meyer, G. Bond-Order Discrimination by Atomic Force Microscopy. *Science* **2012**, *337*, 1326–1329.
33. Kawai, S.; Sadeghi, A.; Feng, X.; Lifen, P.; Pawlak, R.; Glatzel, T.; Willand, A.; Orita, A.; Otera, J.; Goedecker, S. Obtaining Detailed Structural Information about Supramolecular Systems on Surfaces by Combining High-Resolution Force Microscopy with *ab Initio* Calculations. *ACS Nano* **2013**, *7*, 9098–9105.
34. Hipps, K. W.; Scudiero, L.; Barlow, D. E.; Manning, P.; Cooke, J. A Self-Organized 2-Dimensional Bifunctional Structure Formed by Supramolecular Design. *J. Am. Chem. Soc.* **2002**, *124*, 2126.
35. Moll, N.; Schuler, B.; Kawai, S.; Xu, F.; Peng, L.; Orita, A.; Otera, J.; Curioni, A.; Neu, M.; Repp, J.; *et al*. Image Distortions of a Partially Fluorinated Hydrocarbon Molecule in Atomic Force Microscopy with Carbon Monoxide Terminated Tips. *Nano Lett.* **2014**, *14*, 6127–6131.
36. Zhang, J.; Chen, P.; Yuan, B.; Ji, W.; Cheng, Z.; Qiu, X. Real-Space Identification of Intermolecular Bonding with Atomic Force Microscopy. *Science* **2013**, *342*, 611–614.
37. Hapala, P.; Kuchin, G.; Wagner, C.; Tautz, F. S.; Temirov, R.; Jelínek, P. The Mechanism of High-Resolution STM-AFM Imaging with Functionalized Tips. *Phys. Rev. B* **2014**, *90*, 085421.
38. Hämäläinen, S. K.; van der Heijden, N.; van der Lit, J.; den Hartog, S.; Liljeroth, P.; Swart, I. Intermolecular Contrast in

Atomic Force Microscopy Images without Intermolecular Bonds. *Phys. Rev. Lett.* **2014**, *113*, 186102.
39. Kaiser, U.; Schwarz, A.; Wiesendanger, R. Magnetic Exchange Force Microscopy with Atomic Resolution. *Nature* **2014**, *446*, 522–525.
40. Bui, T. T. T.; Dahaoui, S.; Lecomte, C.; Desiraju, G. R.; Espinosa, E. The Nature of Halogen···Halogen Interactions: A Model Derived from Experimental Charge-Density Analysis. *Angew. Chem., Int. Ed.* **2009**, *48*, 3838–3841.
41. Bader, R. F. W.; Carroll, M. T.; Cheeseman, J. R.; Chang, C. Properties of Atoms in Molecules: Atomic Volumes. *J. Am. Chem. Soc.* **1987**, *109*, 7968–7979.
42. Bao, Z.; Lovinger, A. J.; Brown, J. New Air-Stable n-Channel Organic Thin Film Transistors. *J. Am. Chem. Soc.* **1998**, *120*, 207–208.
43. Sakamoto, Y.; Suzuki, T.; Kobayashi, M.; Gao, Y.; Fukai, Y.; Inoue, Y.; Sato, F.; Tokito, S. Perfluoropentacene: High-Performance p-n Junctions and Complementary Circuits with Pentacene. *J. Am. Chem. Soc.* **2004**, *126*, 8138–8140.
44. Grimme, S. Semiempirical GGA-Type Density Functional Constructed with a Long-Range Dispersion Correction. *J. Comput. Chem.* **2006**, *27*, 1787–1799.
45. Riley, K. E.; Murray, J. S.; Fanfrlík, J.; Řezáč, J.; Solá, R. J.; Concha, M. C.; Ramos, F. M.; Politzer, P. Halogen Bond Tunability II: The Varying Roles of Electrostatic and Dispersion Contributions to Attraction in Halogen Bonds. *J. Mol. Model.* **2013**, *19*, 4651–4659.
46. Samai, S.; Biradh, K. Halogen···Halogen Interactions in Assembling β-Sheets into 2D Layers in the Bis-(4-halophenylamido)alkanes and their Co-crystals *via* Inter-halogen Interactions. *CrystEngComm* **2009**, *11*, 482–492.
47. Huang, Y. L.; Li, H.; Ma, J.; Huang, H.; Chen, W.; Wee, A. T. S. Scanning Tunneling Microscopy Investigation of Self-Assembled CuPc/F16CuPc Binary Superstructures on Graphite. *Langmuir* **2010**, *26*, 3329–3334.
48. Salzmann, I.; Moser, A.; Oehzelt, M.; Breuer, T.; Feng, X.; Juang, Z.-Y.; Nabok, D.; Valle, R. G. D.; Duhm, S.; Heimel, G.; *et al*. Epitaxial Growth of p-Stacked Perfluoropentacene on Graphene-Coated Quartz. *ACS Nano* **2012**, *6*, 10874–10883.
49. Giessibl, F. J. High-speed Force Sensor for Force Microscopy and Profilometry Utilizing a Quartz Tuning Fork. *Appl. Phys. Lett.* **1998**, *73*, 3956–3958.
50. Giessibl, F. J. Advances in Atomic Force Microscopy. *Rev. Mod. Phys.* **2003**, *75*, 949.
51. Simon, G. H.; Heyde, M.; Rust, H.-P. Recipes for Cantilever Parameter Determination in Dynamic Force Spectroscopy: Spring Constant and Amplitude. *Nanotechnology* **2007**, *18*, 255503.
52. Albrecht, T. R.; Grütter, P.; Horne, D.; Rugar, D. Frequency Modulation Detection Using High-Q Cantilevers for Enhanced Force Microscope Sensitivity. *J. Appl. Phys.* **1991**, *69*, 668.
53. Majzik, Z.; Setvín, M.; Bettac, A.; Feltz, A.; Cháb, V.; Jelínek, P. Simultaneous Current, Force and Dissipation Measurements on the Si(111) 7 $\times$ 7 Surface with an Optimized qPlus AFM/STM Technique. *Beilstein J. Nanotechnol.* **2012**, *3*, 249.
54. Bartels, L.; Meyer, G.; Rieder, K.-H. Controlled Vertical Manipulation of Single CO Molecules with the Scanning Tunneling Microscope: A Route to Chemical Contrast. *Appl. Phys. Lett.* **1997**, *71*, 213–215.
55. Matsuo, D.; Yang, X.; Hamada, A.; Morimoto, K.; Kato, T.; Yahiro, M.; Adachi, C.; Orita, A.; Otera, J. Fluoro-substituted Phenyleneethynylenes: Acetylenic n-Type Organic Semiconductors. *Chem. Lett.* **2010**, *39*, 1300–1302.
56. Horcas, I.; Fernandez, R.; Gomez-Rodriguez, J.; Colchero, J.; Gomez-Herrero, J.; Baro, A. WSXM: A Software for Scanning Probe Microscopy and a Tool for Nanotechnology. *Rev. Sci. Instrum.* **2007**, *78*, 013705.
57. Kresse, G.; Hafner, J. *Ab Initio* Molecular Dynamics for Liquid Metals. *Phys. Rev. B* **1993**, *47*, 558–561.
58. Kresse, G.; Hafner, J. *Ab Initio* Molecular-Dynamics Simulation of the Liquid-Metal-Amorphous-Semiconductor Transition in Germanium. *Phys. Rev. B* **1994**, *49*, 14251–14269.
59. Kresse, G.; Furthmüller, J. Efficiency of *ab-Initio* Total Energy Calculations for Metals and Semiconductors Using a Plane-Wave Basis Set. *Comput. Mater. Sci.* **1996**, *6*, 15–50.
60. Kresse, G.; Furthmüller, J. Efficient Iterative Schemes for *ab Initio* Total-Energy Calculations Using a Plane-Wave Basis Set. *Phys. Rev. B* **1996**, *54*, 11169–11186.
61. Genovese, L.; Neelov, A.; Goedecker, S.; Deutsch, T.; Ghasemi, S. A.; Willand, A.; Caliste, D.; Zilberberg, O.; Rayson, M.; Bergman, A.; *et al*. Daubechies Wavelets as a Basis Set for Density Functional Pseudopotential Calculations. *J. Chem. Phys.* **2008**, *129*, 014109.
62. Hartwigsen, C.; Goedecker, S.; Hutter, J. Relativistic Separable Dual-Space Gaussian Pseudopotentials from H to Rn. *Phys. Rev. B* **1998**, *58*, 3641–3662.
63. Willand, A.; Kvashnin, Y. O.; Genovese, L.; Vázquez-Mayagoitia, Á; Deb, A. K.; Sadeghi, A.; Deutsch, T.; Goedecker, S. Norm-Conserving Pseudopotentials with Chemical Accuracy Compared to All-Electron Calculations. *J. Chem. Phys.* **2013**, *138*, 104109.
64. Blöchl, P. E. Projector Augmented-Wave Method. *Phys. Rev. B* **1994**, *50*, 17953–17979.
65. Kresse, G.; Joubert, D. From Ultrasoft Pseudopotentials to the Projector Augmented-Wave Method. *Phys. Rev. B* **1999**, *59*, 1758–1775.
66. Caliste, D.; *et al*. *V Sim Visualization Sofware*; CEA-INAC: Grenoble, France, http://inac.cea.fr/L_Sim/V_Sim.
67. Momma, K.; Izumi, F. VESTA 3 for Three-Dimensional Visualization of Crystal, Volumetric and Morphology Data. *J. Appl. Crystallogr.* **2011**, *44*, 1272–1276.